Volume 8, Issue 6, 2018, 3751 - 3757 ISSN 2069-5837

Biointerface Research in Applied Chemistry

www.BiointerfaceResearch.com

Original Research Article Open Access Journal

Received: 22.04.2018 / Revised: 10.11.2018 / Accepted: 20.11.2018 / Published on-line: 15.12.2018

Solution based PEG and PVP capped maghemite–reduced graphene oxide nanocomposites: cell viability study

Atanu Naskar [1], Susanta Bera [1], Rahul Bhattacharya [2], Sib Sankar Roy [2], Sunirmal Jana [1,*]

[1]Sol-Gel Division, CSIR-Central Glass and Ceramic Research Institute, 196 Raja S.C. Mullick Road, Jadavpur, Kolkata 700032, India.
[2]Cell Biology & Physiology Division, CSIR-Indian Institute of Chemical Biology, 4 Raja S.C. Mullick Road, Jadavpur, Kolkata 700032, India

*corresponding author e-mail address: ***sjana@cgcri.res.in, janasunirmal@hotmail.com***

ABSTRACT

We report low temperature solution process based synthesis of polyethylene glycol (PEG) and polyvinyl pyrrolidone (PVP) capped maghemite (γ-Fe_2O_3)–reduced graphene oxide (rGO) nanocomposites (IGPG and IGPP) and their comparative quantitative cell viability (CV) study on human OAW42 ovarian cancer cells. Initially, γ-Fe_2O_3–rGO (IG) nanocomposite was prepared and the IG was capped separately with PEG and PVP for obtaining IGPG and IGPP, respectively. The presence of γ-Fe_2O_3 nanoparticles and organics in the nanocomposites was confirmed by X-ray diffraction and transmission electron microscopy studies. The existence of a chemical interaction between the oxygen functionalities of rGO with the organic polymer (PEG/PVP) and maghemite was confirmed by FTIR and Raman spectral studies. Also, thermogravimetric analysis was made to understand the mass loss behavior of the samples. The IGPG showed better CV than IGPP. This observation was explained on the basis of materials properties of the nanocomposites.

Keywords: *Low temperature solution process; γ-Fe_2O_3, graphene; polymer capped nanocomposites; cell viability.*

1. INTRODUCTION

Most metal oxide nanoparticles such as zinc oxide, iron oxide have enormous applications in biomedical fields [1-4]. The research towards obtaining the better efficacy of the nanoparticles for application in living cell systems is still going on and will be continued. This is because the main problem of using the nanoparticles is the rapid particle aggregation as well as particle dissolution [5] in the living cell systems, hindering the main function of the nanoparticles. Right now, there are several ways to mitigate the problem. One of the effective ways is the capping of the nanoparticles with biocompatible organics like polymers [6] or graphene derivatives [7]. The main advantage of this capping process is that it provides a hydrophilic group to the nanocomposite which could conjugate with any cell system [6]. For this reason, the nanocomposite also becomes water soluble and stable in physiological solutions [3], which is very much desirable for any nanocomposite to function in a cellular system. Reduced graphene oxide (rGO) is a biocompatible material [1-2] which could couple with many metal oxides including zinc oxide, iron oxide [3-4, 8-9]. But the major concern is their aggregation in salt or biological solutions which are undesirable for cell study [10]. In this regard, the modification of its surface could be an important aspect of enhancing the biocompatibility of rGO [11]. Polyethylene glycol (PEG), polyvinyl pyrrolidone (PVP), poly vinyl alcohol (PVA), poly acryl amide (PAM), poly acrylic acid (PAA), poly ethylene oxide (PEO) are some of the known organic polymers, already been investigated [12] on the surface of many metal oxides (ZnO, CeO_2, TiO_2, Fe_3O_4 and Al_2O_3) in aqueous suspension which prevents agglomeration [12]. However, due to the ordered chain structure of PEG and PVP, these could easily be absorbed on γ-Fe_2O_3-rGO nanocomposite surface [13]. Its hydrophilic groups of these polymers could also help the nanoparticles to become water soluble and stable in the physiological medium [6].

Among the nanoparticles, γ-Fe_2O_3 is the widely studied nanoparticles for magnetic resonance imaging (MRI), magnetic fluid hyperthermia, controlled drug delivery systems, cancer therapy and so on [3]. In general, it is regarded as biocompatible. Being nanoparticles, the size of γ-Fe_2O_3 may be equal to the size of the proteins which is desirable for any kind of cell study. Thus, the possibility of interaction with the cell system particularly with the nucleus is more for nanoparticles [14]. However, the toxicity of a particle increases in nano regime [15]. The reason behind this increased toxicity may be due to its high surface to volume ratio [15]. There is also no literature report on comparative cell viability study on polymer capped nanocomposites especially for PEG /PVP capped γ-Fe_2O_3-reduced graphene oxide (rGO).

In the present work, we have tried to address the aforementioned problem by making a γ-Fe_2O_3-reduced graphene oxide (rGO) nanocomposite capping with the organic polymer (PEG/PVP) which form stable material in a biological medium like in the living cells. We also made a comparative study regarding the PEG and PVP capped γ-Fe_2O_3-rGO nanocomposites. The novelty of this study is the use of single surfactant in precursor medium which has been used for the synthesis of γ-Fe_2O_3 and also for the reduction of GO to rGO. Materials characterizations and a comparative cell viability study on human OAW42 ovarian cancer cells has been performed systematically and found that PEG capped γ-Fe_2O_3-reduced graphene oxide is a potential material for the biomedical application.

2. EXPERIMENTAL

2.1. Synthesis of γ-Fe_2O_3 (IO) and γ-Fe_2O_3-rGO nanocomposite (IG). Graphene oxide (GO) was prepared by adopting a modified Hummer's method **[**1**]**. For this purpose, a fixed amount (50 mg) of as-synthesized GO was uniformly dispersed in deionized water (50 ml) under ultrasonication for ~2 h duration. The details have already given in our previous reports [2]. In another solution, 2.5 g of Iron(III) nitrate nonahydrate ($Fe(NO_3)_3.9H_2O$, Merck, ≥98%) was uniformly dispersed in 200 ml of deionized water by continuous stirring. Then, the GO that already dispersed in deionized water was mixed with the Iron(III) nitrate solution while stirring continuously for about 30 min to form a stable precursor. Further 0.5 g of $NaBH_4$ in 25 ml of 3.5 % NH_4OH solution was added to the aliquot for the formation of γ-Fe_2O_3-rGO (IG) nanocomposite. Subsequently, the precursors were kept stirring at ~ 100°C for 2 h for the formation of IG nanocomposite. The solid materials were then separated out by centrifugation. Finally, the products were washed with double distilled water and ethanol, followed by centrifugation for several times. Finally, the samples were dried in an air oven at ~60°C for 3 h. Similar procedure was adopted for the synthesis of γ-Fe_2O_3 nanoparticles (IO) without using GO which has already been reported previously [16].

2.2. Synthesis of PEG coupled γ-Fe_2O_3-rGO (IGPG) and PVP coupled γ-Fe_2O_3-rGO (IGPP) nanocomposites. For the preparation of IGPG nanocomposite [6], 0.05 g of as-prepared γ-Fe_2O_3-rGO nanocomposite (IG) and 0.20 g of polyethylene glycol (PEG-2000, Merck Schuchardt) (IG : PEG =1:4) were dispersed in 30 mL of deionized water. The dispersed material was ultrasonicated for 60 min duration. Then, the mixture was kept at 50°C for 60 min under starring condition. The product was separated by centrifugation and washed the material with de-ionized water and ethanol for 3 times repeatedly, to remove the superfluous PEG. Finally, the washed sample was kept for 3 h in an air oven at 60°C for drying. A similar procedure was adopted for the synthesis of γ-Fe_2O_3-rGO-PVP nanocomposite (IGPP) where IG to PVP weight ratio was kept fixed to 1:4.

3. CHARACTERIZATIONS

3.1. Materials.

X-ray diffraction (XRD) study of the samples was performed by X-ray diffractometer (Bruker D8 Advance with DAVINCI design X-ray diffraction unit) with nickel filtered CuK_α radiation source (λ = 1.5418 Å) in the 2θ range, 5° - 80°. FTIR spectral study was carried out by using Thermo Electron Corporation, USA makes FTIR spectrometer (Nicolet 5700). For each experiment, the number of scans was fixed at 100 (wavenumber resolution, 4 cm^{-1}). Raman spectra of graphene based samples (IG, IGPG, and IGPP along with precursor GO) were recorded from micro-Raman (Renishaw inVia Raman microscope). An argon ion laser with an incident wavelength of 514 nm was used as an excitation source for the measurement. A Netzsch STA 409 C/CD thermoanalyzer was used for thermogravimetric analysis (TG-DTA) of the composite using Al_2O_3 as a reference maintaining the heating rate of 10 K/min in air atmosphere. For the TG-DTA run, a maximum temperature was chosen up to 700°C. Transmission electron microscopy (TEM) measurement of the samples was done by FEI Company made (Tecnai G2 30.S-Twin, Netherlands) machine at an accelerating voltage of 300 kV. Carbon coated 300 mesh Cu grids were used for placement of the samples.

3.2. Cytotoxicity study.

This study was performed using IO, IG, IGPG and IGPP samples with their varying concentrations on human OAW42 ovarian cancer cells procured from ATCC, USA. We used Dulbecco's modified eagles medium (DMEM, Gibco, USA), fetal bovine serum (FBS, Gibco, USA), PenStrep (Gibco, USA) and MTT (3-[4,5-dimethylthiazol-2-yl]-2,5- diphenyl tetrazolium bromide, Sigma, USA) as necessary chemicals and reagents for the study.

3.2.1. Cell culture. Human OAW42 ovarian cancer cells were cultured in DMEM (Gibco) supplemented with 10% fetal bovine serum (FBS) and antibiotic (1% penicillin/streptomycin) in 5% CO_2 at 37°C. The cells from exponentially growing cultures were used for this experiment.

3.2.2. Measurement of *in vitro* cellular cytotoxicity, MTT assay. The MTT assay was done to estimate the viable cells. In a brief process, OAW42 (10^4 cells per well) were seeded on to a flat bottom 96-well plate and incubated at 37°C in 5% CO_2. Cells were treated with or without (i.e. vehicle control) nanocomposite at their varying concentrations, ranging from 0 to 200 μg/ml and kept for 24 h. Finally, it was subjected to MTT assay. Then, 20 μl of MTT (5 mg/ml) was added to each well. After 4 h of incubation, the media was removed and cells were dispersed in 100 μl of dimethyl sulphoxide (DMSO) solvent. Absorbance spectra of the samples were measured at 595 nm wavelength by Qualigens plate reader-96 well. The cell viability values were expressed in percentages with respect to the control values.

4. RESULTS AND DISCUSSION

4.1. X-ray diffraction (XRD). Figure 1 displays the XRD patterns of as-synthesized GO, γ-Fe_2O_3 (IO), γ-Fe_2O_3-rGO (IG), γ-Fe_2O_3–rGO–PEG (IGPG) and γ-Fe_2O_3–rGO–PVP (IGPP) nanocomposites. In this figure, the XRD pattern of GO shows [2] a strong intensity diffraction peak (2θ) at ~10.1° along with a distinct peak appears at ~42.4° (weak intensity), could characterize

the GO with its crystal planes (002) and (100), respectively. However, in this solution synthesis process, the use of $NaBH_4$ in the precursor helped GO to convert it into reduced graphene oxide, rGO [17] and consequently, all these peaks assigned for GO were found to be disappeared in IG, IGPG and IGPP nanocomposite samples. It was further noted that the, XRD peaks of as-synthesized IO, IG, IGPG, and IGPP were fully matched with the spinel structure γ-Fe_2O_3 [JCPDS 39-1346], implying that the crystal structure of γ-Fe_2O_3 was unaffected after capping IO/IG with the organic polymer (PEG/PVP). The average crystallite size (D) of γ-Fe_2O_3 was estimated [2] along (311) crystal plane of γ-Fe_2O_3 by using Debye-Scherrer's equation (1).

$$D = k\lambda / \beta \cos\theta \qquad (1),$$

where k is proportionality constant (k = 0.89), λ is the wavelength of X-ray (1.5406 Å), β is the FWHM (full width at half maximum) of the peak of maximum intensity in radians, θ is the diffraction angle.

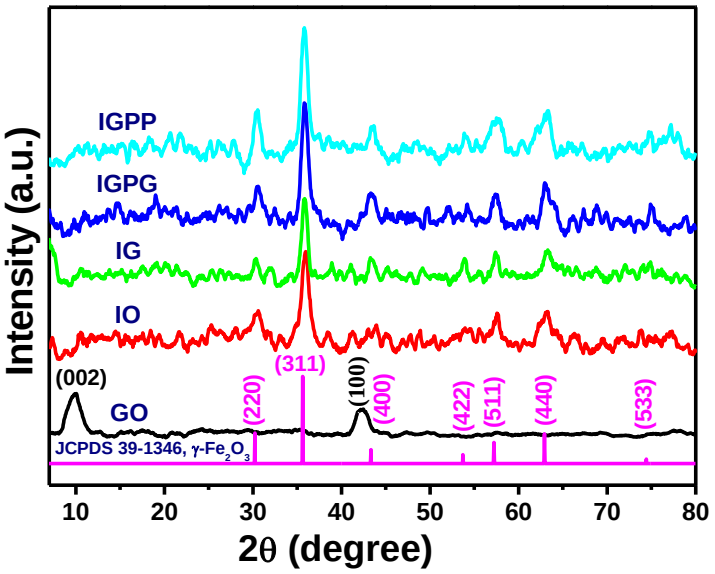

Fig. 1. XRD patterns of IO, IG, IGPG and IGPP samples along with as-synthesized GO.

The measured 'D' values of γ-Fe_2O_3 in IO, IG, IGPG and IGPP samples were ~ 11.0 nm, ~ 9.5 nm, ~ 9.5 nm and ~ 9.5 nm, respectively. Thus, the crystallite size of γ-Fe_2O_3 in IG was found to be decreased after loading of GO [6] but remained identical after capping with PEG or PVP. Therefore, no effect on the change of crystallite size of γ-Fe_2O_3 was found in IGPG or IGPP. This result could indirectly mean that the capping of rGO could completely take place. During conversion of GO to rGO, the oxygen functional groups including hydroxyl groups of GO drastically reduced as confirmed by FTIR, Raman spectral studies (given later). In addition, exfoliation/breaking of graphene layers could create higher structural defects in graphene moiety which would generally be occurred due to chemical interaction/complexation with the available functional groups of rGO with polymer PEG/PVP) / inorganic moiety (γ-Fe_2O_3) [6]. This whole scenario of reduction and complexation could lead to produce larger surface area in the graphene based nanocomposites [6]. The grain growth of nano γ-Fe_2O_3 could be prevented due to capping of rGO through chemical interaction with the nanocrystals [6]. This assumption could be justified as we obtained similar crystallite size of γ-Fe_2O_3 in IGPG and IGPP nanocomposites. It is also noted that PEG and PVP could interact with the available functional groups of rGO as well as the bare surface of γ-Fe_2O_3 [6].

4.2. Thermal analysis. Thermogravimetric analysis (Fig. 2) was implemented to determine the mass loss behaviour of IO, IG, IGPG and IGPP samples. The presence of different organic contents was obtained from the TG curves of the nanocomposites. The thermal analysis showed that at about 500°C temperature, the TG curve of all the samples became parallel to the temperature axis. However, the total mass loss at that temperature was found to be varied greatly, signifying the different content of organics present in the nanocomposites. In this respect, we obtained ~6% mass loss in IO whereas the loss rose to about 13% was seen in IG nanocomposite. Thus, the extra mass loss in IG could be considered due to adsorbed / bonded waters [6]. Hence, the content of rGO could be ~7% in rGO-γ-Fe_2O_3 (IG) nanocomposite. On the other hand, from the total mass loss of ~ 22% and ~24% as observed from their corresponding TG curves, the content of PEG and PVP would be ~9% and ~11% in IGPG and IGPP, respectively. Therefore, this simple thermal analysis indirectly confirmed the PEG and PVP could form the nanocomposites of rGO-γ-Fe_2O_3-PEG (IGPG) and rGO-γ-Fe_2O_3-PVP (IGPP), respectively, were developed *in situ* from IG nanocomposite.

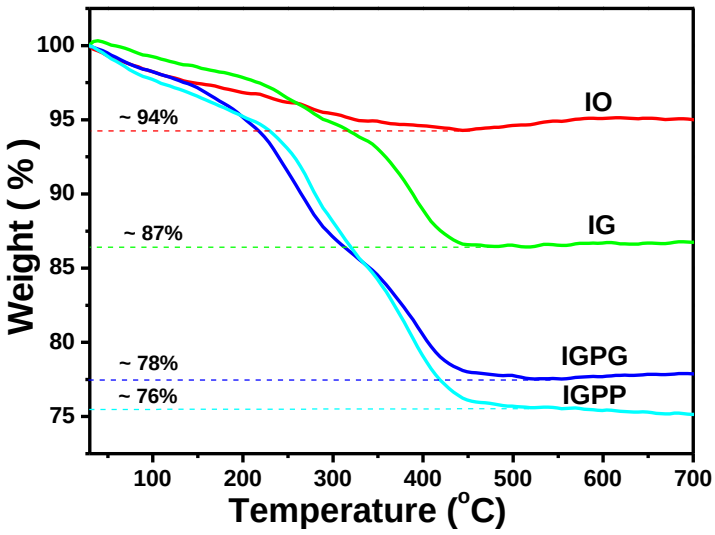

Fig. 2. TG curves of IO, IG, IGPG and IGPP samples.

4.3. FTIR spectra. FTIR vibrational spectra (Fig. 3) were measured for different nanocomposites (IO, IG, IGPG, and IGPP) as well as as-synthesized GO in the spectral range of 4000-400 cm^{-1}. The FTIR spectra not only revealed the chemical interaction/complexation between the available oxygen functional groups of rGO with inorganic nanoparticles (γ-Fe_2O_3) but also supported the presence of chemically interacted PEG/PVP in γ-Fe_2O_3-rGO-PEG (IGPG)/γ-Fe_2O_3-rGO-PVP (IGPP) nanocomposites. In GO, the FTIR peaks appeared at 1730, 1620, 1210, and 1050 cm^{-1} could be assigned to COOH stretching vibrations in carboxylic acid groups, skeletal vibrations of unoxidized graphitic domains, C–OH stretching, and C–O stretching, respectively [2]. It was interesting to note that all the peaks of GO were found to be very weak in intensity or nearly

disappeared in IG, IGPG and IGPP samples, implies the transformation of GO to rGO took place [2]. This transformation of rGO also was confirmed by the appearance of a new peak observed at ~1565 cm^{-1} in IG, IGPG and IGPP samples. It is worthy to note that no such peak was found in GO sample. Irrespective nanocomposite type, the presence of γ-Fe_2O_3 was also revealed from the existence of Fe–O vibrations at ~570 and ~630 cm^{-1} [18] and the result obviously supported the XRD analysis (Fig. 1) of the samples. The purity of the γ-Fe_2O_3 phase could also be confirmed by the fact that magnetite (Fe_3O_4) has no FTIR vibration above 600 cm^{-1} [19]. It is to be mentioned that a prominent shoulder appeared at 3432 cm^{-1} could attribute to the presence of hydroxyl groups in all the samples [6]. On the other hand, two new peaks appeared in the FTIR spectra of IGPG at ~1395 cm^{-1} and ~2920 cm^{-1} could be attributed to the presence of PEG in the nanocomposites [6], interacted with γ-Fe_2O_3-rGO moiety. The presence of chemically interacted PVP would also be recognized from the appearance of FTIR peak at ~1650 cm^{-1} in IGPP [20].

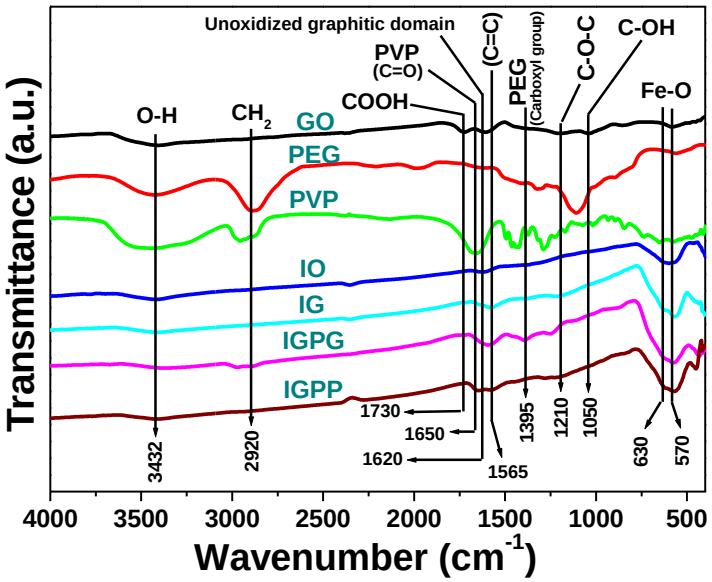

Fig. 3. FTIR spectra of IO, IG, IGPG, and IGPP along with as-synthesized GO.

4.4. Raman spectra. To confirm the interaction happened between γ-Fe_2O_3, rGO, PEG/PVP in the nanocomposites and to study the structural changes/layer by layer exfoliations in graphene moiety of rGO, micro-Raman spectral study (Fig. 4) was performed. Two prominent peaks were observed at ~1350 cm^{-1}, assigned to D band (defect) and at ~1595 cm^{-1}, assigned to G band (graphene) [2] in GO and graphene based nanocomposites i.e. IG, IGPG, and IGPP. The D band could be originated due to exfoliation/breaking of graphene layers whereas G band could be due to E_{2g} phonon of sp^2 carbon atoms in graphene moiety [1]. The intensity ratio (I_D/I_G) of D and G Raman bands in different nanocomposites was measured. The intensities of *D* and *G* bands were designated as I_D and I_G, respectively. A relative increment in I_D/I_G value in IG sample compared to precursor GO (Fig. 4) was obtained from its Raman spectrum and this could be associated with the exfoliation/breaking of graphene layers due to chemical interaction/complexation with the inorganic moiety [21]. It is worthy to note that the I_D/I_G ratio was found to be changed further after incorporation of PEG and PVP in IG forming IGPG and IGPP, respectively. This observation could indirectly imply a further chemical interaction that happened between PEG/PVP with IG nanocomposite [6] and the result is fully supported the FTIR spectral analysis (Fig. 3). It is noted that a higher I_D/I_G value in IGPG of 1.60 was found compared to the value (I_D/I_G, 1.23) that obtained in IGPP. Moreover, the shifting of D band in IGPG was higher than IGPP. The observation could obviously indicate the interaction of rGO with PEG in IGPG was much higher than in IGPP. This functional property of IGPG could be useful for the biomedical application (discussed later).

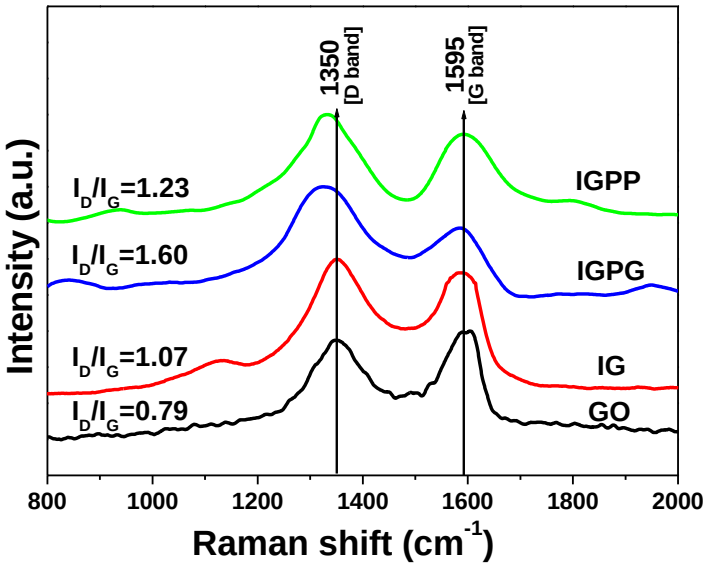

Fig. 4. Raman spectra of GO, IG, IGPG and IGPP samples. Respective I_D/I_G value is embedded in the figure.

4.5. UV-Vis spectra. UV–vis absorption spectra (measured from diffused reflectance spectra with the help of Kubelka–Munk algorithm) of IO, IG, IGPG and IGPP samples are shown in Figure 5. A broad absorption peak in the range of 300–550 nm was observed in all the samples could be related to γ-Fe_2O_3 [22].

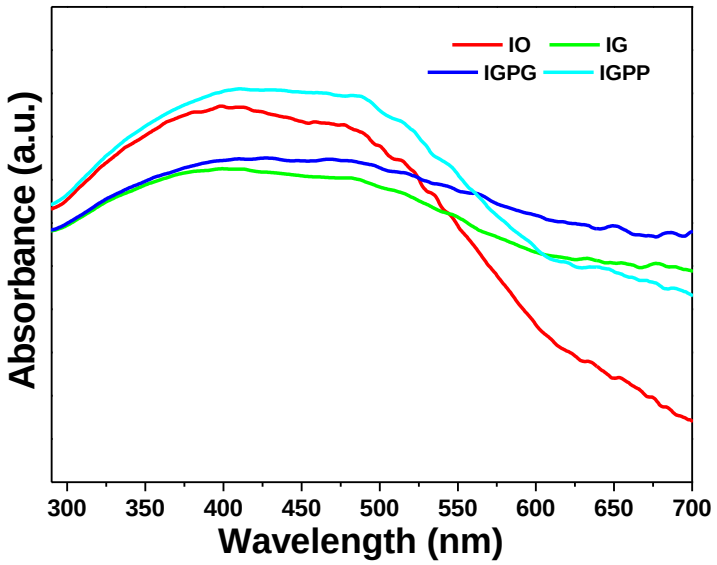

Fig. 5. UV-Visible absorption spectra of IO, IG, IGPG and IGPP samples.

4.6. TEM microstructure. The TEM microstructures of γ-Fe_2O_3 (IO), γ-Fe_2O_3-rGO (IG), γ-Fe_2O_3-rGO-PEG (IGPG) and γ-Fe_2O_3-rGO-PVP (IGPP) are shown in Figure 6. The corresponding

HRTEM images were also given in Figure 6b, Figure 6d, Figure 6f, and Figure 6h, respectively. Figure 6a shows the shape of pure γ-Fe_2O_3 nanoparticles is approximately spherical in shape. The formation of γ-Fe_2O_3 nanoparticles was also confirmed by the corresponding HRTEM image (Fig. 6b). In this respect, the existence of lattice fringes with an interplanar distance of 0.29 nm, corresponds to (220) plane of γ-Fe_2O_3 [23]. The microstructure of γ-Fe_2O_3-rGO (IG) nanocomposite was also shown in Figure 6c where graphene sheet was clearly visible from the appearance of wavy like fringe patterns. The γ-Fe_2O_3 nanoparticles could also be seen in rGO sheet confirming the formation of γ-Fe_2O_3-rGO (IG) nanocomposites. Corresponding HRTEM image (Fig. 6d) also shows the same lattice fringes with an interplanar distance of 0.29 nm corresponds to (220) plane of γ-Fe_2O_3. Microstructure of IGPG and IGPP nanocomposites were also shown in Figure 6e and Figure 6g, respectively where the same type of γ-Fe_2O_3 nanoparticles could be visible in graphene sheet but with less agglomeration. Corresponding HRTEM image (Fig. 6f,h) of the sample also confirmed the presence of γ-Fe_2O_3. The particle size distribution in IO, IG, IGPG and IGPP are shown in the histograms (Insets, Fig. 6a, 6c, 6e and 6g respectively) constructed from their respective TEM images. From the histograms, the measured average particle sizes are ~11.2 nm, ~9.6 nm, ~10.8 nm and ~ 11.4 nm respectively.

Based on XRD (Fig. 1), TG-DTA (Fig. 2), FTIR (Fig. 3), Raman (Fig. 4), UV-Vis (Fig. 5), and TEM (Fig. 6) analyses, a probable formation mechanism and the structure of IGPG/IGPP nanocomposite are given in Scheme 1.

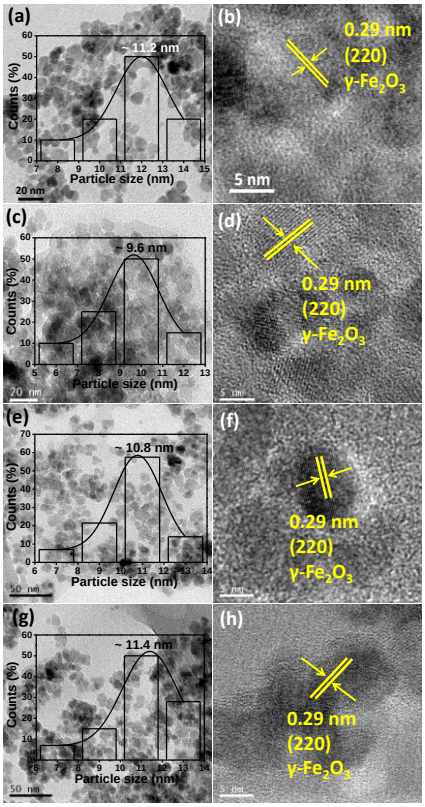

Fig. 6. TEM images of (a) IO, (c) IG, (e) IGPG and (g) IGPP samples. Histograms for particle size distributions are displayed in their insets. HRTEM images of (b) IO, (d) IG, (f) IGPG and (h) IGPP nanocomposites.

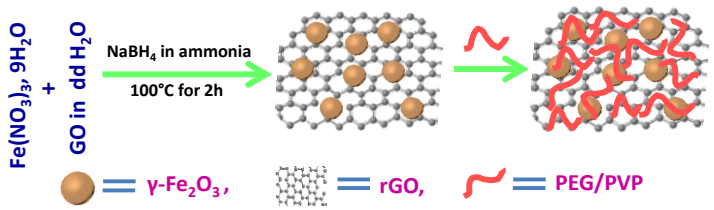

Scheme 1. Proposed mechanism for the formation of PEG/PVP capped γ-Fe_2O_3-rGO (IGPG/IGPP) nanocomposites. In the scheme, dd H_2O means double distilled water.

4.7. *In vitro* cellular cytotoxicity. Measurement of *in vitro* cytotoxicity on human ovarian cancer cell line, OAW42 was done for IO, IG, IGPP and IGPG samples and cell viability percentage (CVP) (Fig. 7) were calculated from the measurement by varying the concentration of respective sample. Each bar graph signifies an average result of three consecutive measurements. It is seen that the CVP decreased in the order of IGPG>IGPP>IG>IO as seen from the figure. It is also significant to note that irrespective of all the doses (μg/ml), IGPG shows always much higher CVP than the other samples. The IGPG nanocomposite shows nearly 80% of viable cells at 50 μg/ml dose with respect to the control. The reason for the higher cytotoxicity of IO nanoparticle could be attributed to the cellular uptake of dissolute ions [24]. Numerous approaches had already been taken by several researchers to prevent this ion dissolution problem [6]. Among which the coupling with reduced graphene oxide (rGO) is obviously an excellent strategy to mitigate the problem [6]. The notable fact over choosing rGO is its biocompatibility towards the cells [6].

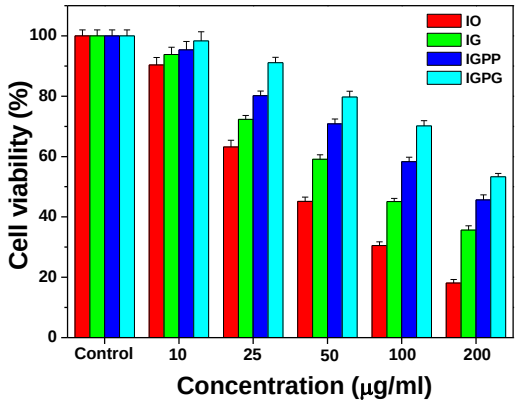

Fig. 7. Cell viability from *in vitro* cellular cytotoxicity, MTT assay of human ovarian OAW42 cell line, for IO, IG, IGPG and IGPP samples with varying concentrations. The error bars represent ±SD (P<0.05).

Figure 7 also shows the CVP of IG is better than IO in all concentrations, which confirms about the ability of rGO to mitigate the problem. Despite its advantages and effectiveness in cell system, there also lies another problem which needs to be resolved. That problem comes within the form of available oxygen functional groups of rGO which could cause some cytotoxicity effect [6]. That's why in our earlier work, PEG was used to resolve this problem in ZnO system [6]. In our present work, we compared the suitability and effectiveness of the biocompatible organic polymers which are generally used for this purpose. From the literatures, we found that PEG and PVP are mostly used for studying the cell viability [6, 25-26]. Moreover, it is also clear from the figure is that the cell viability of IGPG and IGPP is better than IG. Therefore, the higher cell viability in IGPG and IGPP

could be attributed to the coupling of the polymer (PEG or PVP) with γ-Fe_2O_3-rGO nanocomposites. The polymer chemically interacted with the available oxygen functional groups of rGO as well as the bare surface of the inorganic moiety of γ-Fe_2O_3. The interaction could be confirmed from increased I_D/I_G value from Raman spectra (Fig. 4). It is also worthy to mention that both PEG and PVP are water soluble [6, 12] but the higher I_D/I_G value of IGPG to IGPP (Fig. 4) could help to exfoliate the rGO sheet more compare to PVP. That's why the dissolution of ions could be prevented further by IGPG than IGPP. Moreover, the interaction between IG and PEG was much higher than PVP which implies that PEG would be more effective to prevent the oxygen functional groups of rGO in biomedical application.

5. CONCLUSION

Polyethylene glycol (PEG) and polyvinyl pyrrolidone coupled γ-Fe_2O_3-rGO nanocomposites (IGPG and IGPP) were successfully synthesized by adopting facile low temperature solution process. The PEG and PVP found to interact with γ-Fe_2O_3-rGO nanocomposites. From the measurement of in vitro cellular cytotoxicity on human ovarian cancer cell line, OAW42, quantitative cell viability (CV) were obtained by varying the concentration of samples. In this respect, IGPG showed an excellent CV of the cancer cells (nearly ~ 90% of viable cells at 25 μg/ml dose with respect to the control) compare to IGPP sample. An effective role of the biocompatible PEG in association with rGO could enhance the cell viability in IGPG. This simple comparative study could be beneficial for other metal oxide system for biomedical applications.

6. REFERENCES

[1] Bera S., Ghosh M., Pal M., Das N., Saha S., Dutta S. K., Jana S., Synthesis, characterization and cytotoxicity of europium incorporated ZnO–graphene nanocomposites on human MCF7 breast cancer cells, *RSC Adv.*, 4 37479–90, **2014**.

[2] Naskar A., Bera S., Bhattacharya R., Saha P., Roy S.S., Sen T., Jana S., Synthesis, characterization and antibacterial activity of Ag incorporated ZnO–graphene nanocomposites, *RSC Adv.*, 6, 88751–61, **2016**.

[3] Magro M., Baratella D., Bonaiuto E., de A Roger J., Vianello F.Z., New perspectives on biomedical applications of iron oxide nanoparticles, *Curr Med Chem.*, 25(4), 540-555, **2018.**

[4] Sood A., Arora V., Shah J., Kotnala R.K., Jain T.K., Multifunctional gold coated iron oxide core-shell nanoparticles stabilized using thiolated sodium alginate for biomedical applications, *Mater. Sci. Eng. C*, 80, 274-281, **2017**.

[5] Waalewijn-Kool P.L., Ortiz M.D., Straalen N.M.V., Gestel C.A.M. van, Sorption, dissolution and pH determine the long-term equilibration and toxicity of coated and uncoated ZnO nanoparticles in soil, *Environ. Pollut*, 178, 59–64, **2013**.

[6] Naskar A., Bera S., Bhattacharya R., Roy S.S., Sen T., Jana S., Synthesis, characterization and cytotoxicity of polyethylene glycol coupled zinc oxide–chemically converted graphene nanocomposite on human OAW42 ovarian cancer cells, *Polym. Adv. Technol*., 27, 436-43, **2016**.

[7] Kumar K., Loupias L., Canaff C., Morisset S., Pronier S., Morais C., Habrioux A., Napporn T.W., Kokoh K.B., Preparation and electrochemical properties of $NiCo_2O_4$ nanospinels supported on graphene derivatives as earth-abundant oxygen bifunctional catalysts, *ChemPhysChem*., 19, 319-326, **2018**.

[8] Bera S,, Naskar A,, Pal M., Jana S., Low temperature synthesis of graphene hybridized surface defective hierarchical core–shell structured ZnO hollow microspheres with long-term stable and enhanced photoelectrochemical activity, *RSC Adv*., 6 36058–68, **2016**.

[9] Bera S., Pal M., Naskar A., Jana S., Hierarchically structured ZnO-graphene hollow microspheres towards effective reusable adsorbent for organic pollutant via photodegradation process, *J. Alloys Compd*., 669, 177–86, **2016.**

[10] Haute D.V., Liu A.T., Berlin J.M., Coating metal nanoparticle surfaces with small organic molecules can reduce nonspecific cell uptake, *ACS Nano*, 12 (1), 117–127, **2018**.

[11] Cheng Y., Mallavarapu M., Naidu R., Chen Z., In situ fabrication of green reduced graphene-based biocompatible anode for efficient energy recycle, *Chemosphere*, 193, 618-624, **2018**.

[12] Sudha M., Senthilkumar S., Hariharan S.R., Suganthi A., Rajarajan M., Synthesis, characterization and study of photocatalytic activity of surface modified ZnO nanoparticles by PEG capping, *J Sol-Gel Sci Technol*., 65, 301–10, **2013**.

[13] Thirugnanam T., Effect of polymers (PEG and PVP) on sol-gel synthesis of microsized zinc oxide, *J. Nanomater*., 362175, **2013**.

[14] Dam D.H.M., Lee J.H., Sisco P.N., Co D.T., Zhang M., Wasielewski M.R., Odom T.W., Direct observation of nanoparticle cancer cell nucleus interactions, *ACS Nano*, 6, 3318–26, **2012**.

[15] Schrand A.M., Rahman M.F., Hussain S.M., Schlager J.J., Smith D.A., Syed A.F., Metal-based nanoparticles and their toxicity assessment *Wiley Interdiscip. Rev.: Nanomed. Nanobiotechnol*., 2 ,544–68, **2010**.

[16] Heger Z., Cernei N., Blazkova I., Kopel P., Masarik M., Zitka O., Adam V., Kizek R., γ-Fe_2O_3 nanoparticles covered with glutathione modified quantum dots as a fluorescent nanotransporter, *Chromatographia*, 77, 1415–23, **2014**.

[17] Jokar E., Huang Z.Y., Narra S., Wang C.-Y., Kattoor V., Chung C.-C., Diau E.W.-G., Anomalous charge-extraction behavior for graphene-oxide (GO) and reduced graphene-oxide (rGO) films as efficient p-contact layers for high-performance perovskite solar cells, *Adv. Energy Mater*., 8, 1701640, **2018**.

[18] Donadelli J.A., Einschlag F.S.G., Laurenti E., Magnacca G., Carlos L., Soybean peroxidase immobilized onto silica-coated superparamagnetic iron oxide nanoparticles: Effect of silica layer on the enzymatic activity, *Colloids Surf. B*, 161, 654-661, **2018**.

[19] Sun J., Xu B., Mu Y., Ma H., Qu W., Functional magnetic nanoparticles for highly efficient cholesterol removal, *J. Food Sci*., 83, 122-128, **2018**.

[20] Mirzaeei S., Berenjian K., Khazaei R., Preparation of the potential ocular inserts by electrospinning method to achieve the prolong release profile of triamcinolone acetonide, Adv Pharm Bull., 8(1), 21–27, **2018**.

[21] Chandra V., Park J., Chun Y., Lee J.W., Hwang I.-C., Kim K.S., Water-dispersible magnetite-reduced graphene oxide composites for arsenic removal, *ACS Nanno*, 4, 3979–86, **2010.**

[22] Kumar V.B., Marcus M., Porat Z., Shani L., Yeshurun Y., Felner I., Shefi O., Gedanken A., Ultrafine highly magnetic fluorescent γ-Fe_2O_3/NCD nanocomposites for neuronal manipulations, ACS Omega, 3, 1897−1903, **2018.**

[23] Bandhu A., Sutradhar S., Mukherjee S., Greneche J.M., Chakrabarti P.K., Synthesis, characterization and magnetic property of maghemite (γ-Fe_2O_3) nanoparticles and their protective coating with pepsin for bio-functionalization, *Mater. Res. Bull*., 70, 145–54, **2015**.

[24] Zhu X., Tian S., Cai Z., Toxicity assessment of iron oxide nanoparticles in zebrafish (Danio rerio) early life stages, *PLoS One* **7** e46286, **2012**.
[25] Zhang F., Durham P., Sayes C.M., Lau B.L.T., Bruce E.D., Particle uptake efficiency is significantly affected by type of capping agent and cell line, *J. Appl. Toxicol*., 35, 1114–21, **2015.**
[26] Iswarya V., Manivannan J., De A., Paul S., Roy R., Johnson J.B., Kundu R., Chandrasekaran N., Mukherjee A., Mukherjee A., Surface capping and size-dependent toxicity of gold nanoparticles on different trophic levels, *Environ Sci Pollut Res Int*., 23, 4844-58, **2016**.

7. ACKNOWLEDGEMENTS

The authors, AN and SB thankfully acknowledge UGC-RGNF and CSIR, Govt. of India for providing their Ph.D. research fellowships. The authors also acknowledge the help rendered by Nanostructured Materials Division, Bioceramic and Coating Division for Raman spectra and Electron Microscopy Section for microstructural characterizations. The work had been done as an associated research work of 12th Five Year Plan project of CSIR (No. ESC0202).